Tensor Decomposition Analysis for UAV Anomaly Detection

Elizabeth J. Hale *
NASA Ames Research Center, Moffett Field, CA 94035

Portia Banerjee†
KBR, NASA Ames Research Center, Moffett Field, CA 94035

Rajeev Ghimire‡
KBR, NASA Ames Research Center, Moffett Field, CA 94035

Vibrational anomalies can provide valuable insights into the health status of an unmanned aerial vehicle, potentially indicating system degradation including propeller, motor, or sensor damage, as well as environmental anomalies such as strong wind gusts and turbulence. However, many causes for vibrational anomalies are not related to vehicle health, such as sharp shifts in velocity or direction of flight. Thus, depending strictly on vibration signals to detect anomalies can result in false positives for failures. Hence, it is important to include additional telemetries in detecting and diagnosing in-flight anomalies. This paper considers an approach to anomaly detection based on tensor decompositions that incorporates information from vibration signals, as well as additional flight data such as velocity, current draw, voltage drop, and attitude. Using experimental flight data collected by the University of Notre Dame, we construct third-order tensors then apply the CANDECOMP/PARAFAC decomposition to identify trends within each flight and classify flights as nominal or anomalous.

I. Introduction

With the use of unmanned aerial vehicles (UAVs) on the rise, it is increasingly important to detect and diagnose different failure modes. Such aircraft have a wide variety of uses, such as military applications, aerial photography, and disaster relief, including wildfire detection and mitigation. Due to their flexibility in size and the ability to be controlled from a remote location, UAVs offer many advantages over traditional manned aircraft. However, often times taking advantage of the smaller sizes available in UAVs means sacrificing payload capacity. In particular, this can create challenges in dealing with aircraft failures due to the inability to utilize redundant systems typically found in full-size aircraft. Therefore, it is critical to develop effective health-monitoring systems to ensure that appropriate measures such as flight termination, trajectory alterations, and/or repairs take place prior to system failures.

Fault detection and diagnosis for UAVs can focus on many aircraft components and provides valuable insight into the state of health of the aircraft, and vibration analysis is becoming especially important in this area. This approach can be used to detect a wide range of anomalies in flight, including propeller degradation or friction [1–4], bearing faults [5], excess payload [6, 7], and even disruptions due to high wind [6].

Many different approaches have been implemented to characterize and classify vibration signals arising from anomalies in flight. Frequency analysis is a particularly popular method, as changes in the cyclic behavior of the motors or propellers can reveal information about the health of these components. Such approaches were implemented in [1, 3–5] through the use of the Fourier transform to examine frequency components present in the vibrations, while [2] focused on wavelet based analysis to preserve precision in the time domain. However, it can be challenging to sample such signals at sufficiently high frequencies to capture such features without the use of specialized payloads [6]. As a result, time series methods such as k-means clustering are also valuable tools for isolating signals resulting from faults [6, 8]. Such time-based approaches to anomaly detection have been applied in a variety of settings outside of UAVs. Liu et al. [9] offer a survey of machine-learning based techniques for anomaly detection, as well as introduce the isolation forest approach. Shin et al. [10] use a tensor decomposition based approach to capturing high dimensional data, enabling them to leverage information from multiple parameters at a time.

*NASA Pathways Intern, Intelligent Systems Division, elizabeth.j.hale@nasa.gov, Corresponding author.
†Research Engineer, Intelligent Systems Division, portia.banerjee@nasa.gov, AIAA Member.
‡Research Engineer, Intelligent Systems Division, rajeev.ghimire@nasa.gov, AIAA Member.

Also of interest is understanding the impact of environmental anomalies; in particular, many recent studies have considered how wind might affect UAVs. For example, Mohamed et al. [11] analyze the effects of wind gusts near buildings on rotary and fixed wind aircraft through simulations. Lei et al. [12] consider the impact of wind on the aerodynamic performance of a quadcopter during hover. In the context of vibration analysis, Banerjee et al. [6] use k-means clustering to classify vibration signals in quadcopters related to wind gust strength. Strong winds pose a threat to aircraft health and safety, as well as successful trajectory/mission completion, so it is critical that these effects are well understood.

We look to continue analyzing the relationship between wind and vibration signals. However, due to the large number of causes for changes in the vibration signals, it is desirable to consider additional parameters beyond vibration. For example, the tests performed in [6] showed increases in vibration magnitudes can result from high winds or could simply be due to the increase of speed in the aircraft. With this in mind, we implement the tensor-based method proposed in [10], which was specifically developed in the context of satellite telemetries to mitigate the issues of false positives that result from the use of a single threshold applied to one parameter at a time. Instead, this method incorporates information across all parameters of interest to identify anomalies and minimize false positives by constructing a third-order tensor using summary statistics from several telemetries then applying a CANDECOMP/PARAFAC (CP) decomposition to identify anomalous moments of operation.

This document is organized as follows. We begin with an overview of relevant tensor analysis notation, definitions, and theory in Section II, followed by an overview of the Integrative Tensor-based Anomaly Detection (ITAD) method in Section III. We then describe the data collected by the University of Notre Dame used in this analysis in Section IV and apply ITAD to the data set and discuss the results in Section V. Finally, we conclude the study in Section VI with some observations about the results and the data set and identify potential next steps to continue these analyses.

II. Tensors and Tensor Decomposition Background

Tensors offer a way to represent high dimensional data, commonly thought of as generalizations of matrices and vectors (see Fig. 1). This makes them a popular option for working with data with features that are ineffective or even impossible to analyze in one or two dimensions, as information can be masked or completely lost when collapsed into a vector or matrix.

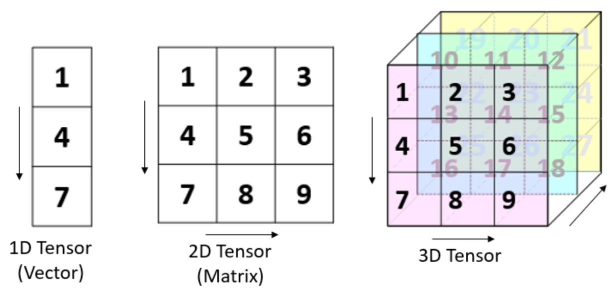

Fig. 1 Tensors are higher dimensional analogs of matrices and vectors

However, in spite of the advantages offered by representing data in higher dimensions, an immediate challenge arises with the large volume of data that can be stored in this way. For example, a $50 \times 100 \times 20$ 3-dimensional tensor contains 100,000 data points. Moreover, while this structure preserves relationships inherent in each dimension, extracting key features from the data can be difficult. To address this, tensor decompositions were developed. Such decompositions can be thought of as higher-dimensional analogs of matrix decompositions, as they share the purpose of offering more efficient storage and capturing overarching features in the data set.

Over the last several years, many contributions have been made to the field of tensor analysis and decompositions. Interestingly enough, while the field is inherently mathematical in nature, for nearly a century much of the foundational work was done in interdisciplinary applications including chemistry, neuroscience, signal processing, and psychology. However, over the last decade, a big push has occurred in the mathematical community to formalize the work done in this area. Much of this has occurred thanks to the work of Kolda and Bader [13], who in 2009 wrote a comprehensive paper summarizing much of the work done in this field, including operations, theory, and tensor-based algorithms, and also developed a corresponding MATLAB package implementing related operations and algorithms. With this in mind, we use their notation and definitions throughout this report, and refer the reader to [13] for additional details on the topics contained in this section.

We begin with common definitions and notations related to tensors. The number of dimensions of a tensor is called its order, while each dimension is frequently referred to as a mode. For the purposes of this analysis, it is sufficient to work with order 3 tensors. However, it should be noted that tensors may be of any order and all tensor operations and algorithms shown here can be extended to higher dimensions.

We will denote tensors with upper-case, calligraphic letters, for example, $\mathcal{X}$; matrices will be denoted with uppercase boldface letters, for example, $\mathbf{A}$; and vectors will be denoted with lowercase boldface letters, for example $\mathbf{x}$. Finally, the elements of the aforementioned objects will be denoted in lower case with appropriate subscripts. For example, the element of $\mathcal{X}$ in the (i, j, k) position will be represented by x_{ijk}.

There are several operations similar to those used with matrices that can be applied in this higher-dimensional setting. Usually, the norm of a tensor is its Frobenius norm. That is, for a 3-way tensor $\mathcal{X} \in \mathbb{R}^{I \times J \times K}$

$$\|\mathcal{X}\| = \sqrt{\sum_{i=1}^{I} \sum_{j=1}^{J} \sum_{k=1}^{K} x_{ijk}^2}. \tag{1}$$

Also, we recall that the outer product of two vectors results in a matrix. In particular, for column vectors $\mathbf{a} \in \mathbb{R}^I$ and $\mathbf{b} \in \mathbb{R}^J$, their outer product is defined as $\mathbf{a} \circ \mathbf{b} = \mathbf{a}\mathbf{b}^T$. Componentwise, $(\mathbf{a} \circ \mathbf{b})_{ij} = a_i b_j$. Analogously, taking the outer product of n vectors results in an n-dimensional tensor. For example, letting $\mathbf{c} \in \mathbb{R}^K$, $\mathbf{a} \circ \mathbf{b} \circ \mathbf{c}$ is a 3-way tensor in $\mathbb{R}^{I \times J \times K}$ with components determined by $(\mathbf{a} \circ \mathbf{b} \circ \mathbf{c})_{ijk} = a_i b_j c_k$. A visual representation of this is given in Fig. 2.

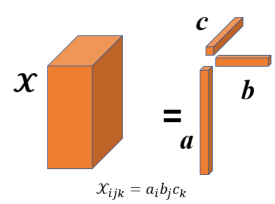

Fig. 2 The outer product of three vectors is a tensor.

The outer product induces the notion of the rank of a tensor. The outer product of any three vectors creates a 3-way tensor. If a given tensor can be written as a single outer product of vectors, we say it has rank one. However, not every tensor can be written as a single outer product of vectors. However, tensors can be written as the sum of outer products of vectors. The smallest number of components R needed to write a given tensor as the sum of outer products of vectors is called its rank. In some regards, this notion of rank is analogous to the rank of a matrix. For example, when thinking of the singular value decomposition of a matrix written as the sum of outer products, the rank of the matrix is equal to the number of terms in the sum. However, there are fundamental differences in how rank behaves relative to the size of the tensor. That is, the size of the dimensions of the tensor do not directly give upper bounds on the rank, and in many instances, the relationship between the size of the tensor and the rank of the tensor is unknown [13]. In addition, unlike matrices, there is no algorithm to determine the rank of a tensor; in fact this problem is NP hard [14].

Nonetheless, writing a tensor as a sum of outer products is one of the most popular tensor decompositions. Tensor decompositions were first introduced by Hitchcock as early as 1927 [15]. But this specific approach was popularized as the CANDECOMP/PARAFAC (CP) decomposition by Carroll and Chang [16] and Harshman [17] independently in 1970. In this decomposition, a tensor, $\mathcal{X}$ is written as the sum of outer product of vectors, as shown in Fig. 3. We will refer to each term $1, 2, \ldots, R$ as the factors of the decomposition.

It is common to require that $\mathbf{a}_r$, $\mathbf{b}_r$, and $\mathbf{c}_r$ have unit length and to incorporate a vector containing appropriate scaling values, λ. Ultimately, $\mathcal{X}$ is written as

$$\mathcal{X} = \sum_{r=1}^{R} \lambda_r \mathbf{a}_r \circ \mathbf{b}_r \circ \mathbf{c}_r \tag{2}$$

(note that λ_r is a scalar). Similar to the matrix setting, if the sum is truncated, we call the resulting tensor a low rank representation of $\mathcal{X}$. It is common to use the Kruskal notation

$$\mathcal{X} = [\![\lambda; \mathbf{A}, \mathbf{B}, \mathbf{C}]\!], \tag{3}$$

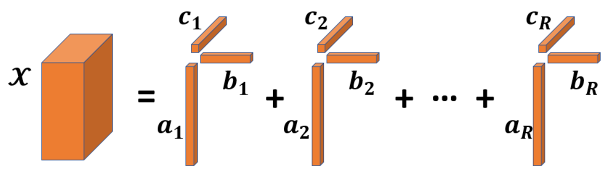

Fig. 3 Tensors can be expressed as a sum of outer products

for this decomposition, where $\mathbf{A} \in R^{I\times R}$, where $\mathbf{A}$ is formed by horizontally concatenating $\mathbf{a}_1, \mathbf{a}_2, \ldots, \mathbf{a}_R$, with analogous constructions for $\mathbf{B} \in \mathbb{R}^{R\times J}$ and $\mathbf{C} \in \mathbb{R}^{K\times R}$.

The most popular algorithm for computing the CP decomposition is called CP Alternating Least Squares, or CP ALS. It is based on solving the following optimization problem for a fixed rank R:

$$[\![\lambda; \mathbf{A}, \mathbf{B}, \mathbf{C}]\!] = \operatorname{argmin} \left\| \mathcal{X} - \sum_{r=1}^{R} \lambda_r \; \mathbf{a_r} \circ \mathbf{b_r} \circ \mathbf{c_r} \right\|.$$

The specifics of this algorithm can be found in [13]. The main characteristic of this algorithm is its use of unfolded (or matricized) versions of the tensor and its potential decomposition, which is iteratively updated. In most applications, the iteration terminates when the reconstruction fit, defined as

$$E_R(\mathcal{X}) = \left\| \mathcal{X} - \sum_{r=1}^{R} \lambda_r \; \mathbf{a_r} \circ \mathbf{b_r} \circ \mathbf{c_r} \right\|,$$

no longer changes by more than a specified amount.

III. Integrative Tensor-based Anomaly Detection

Since the CP decomposition of a tensor has the ability to capture key features in high dimensional data set, it is a good candidate for integration into an anomaly detection scheme. Shin et al. [10] implement an anomaly detection method called Integrative Tensor-based Anomaly Detection (ITAD) to detect anomalies in satellite telemetries. In this approach, the authors construct a 3^{rd} order tensor using the time series data of different telemetries from the satellite of interest, perform a CP decomposition of the tensor, then apply clustering techniques to the factor matrix $\mathbf{A}$. In this section, we discuss how a similar approach can be applied with UAV flight data from the University of Notre Dame to incorporate multiple parameters to detect anomalous flights.

In our approach to this method, we construct a tensor that contains temporal information, parameter information, and summary statistics for those parameters. The resulting tensor is 3 dimensional, with the first dimension corresponding to times, the second dimension corresponding to summary statistics, and the third dimension corresponding to the parameter used. We then perform the CP decomposition of the resulting tensor. Recall that the rows of $\mathbf{A}$ correspond to a specific segments of time in the flights; thus we treat them as coordinate points, plotting them and looking for any clustering or distinct behavior in the points corresponding to each flight. The complete process can be seen in Fig. 4 and is explained in detail below. All analysis was performed in MATLAB.

First, an appropriate tensor must be constructed containing the data from all flights of interest. To construct this tensor, we begin with the time series for a single parameter such as vibration. In order to have all the flight information in a single tensor, each flight of interest is concatenated in this time series. Then, within the time series, the data is normalized by dividing by the maximum absolute value in the series. Since different parameters have different ranges of values, normalizing the time series for each parameter prevents parameters with significantly larger values from masking the influence of other parameters. We note that this normalization is taken across all flights within in the time series, with the exception of the voltage. The voltage data is normalized within each flight since each flight had a different starting voltage.

Once normalized, this time series is broken up into blocks of time, either 30s or 15s. The length of time is chosen so that each time block only contains data from one flight. Now, for each block of time, we compute summary statistics. Statistics tested were average, standard deviation, energy, skewness, kurtosis, minimum, quartiles, maximum, and mode;

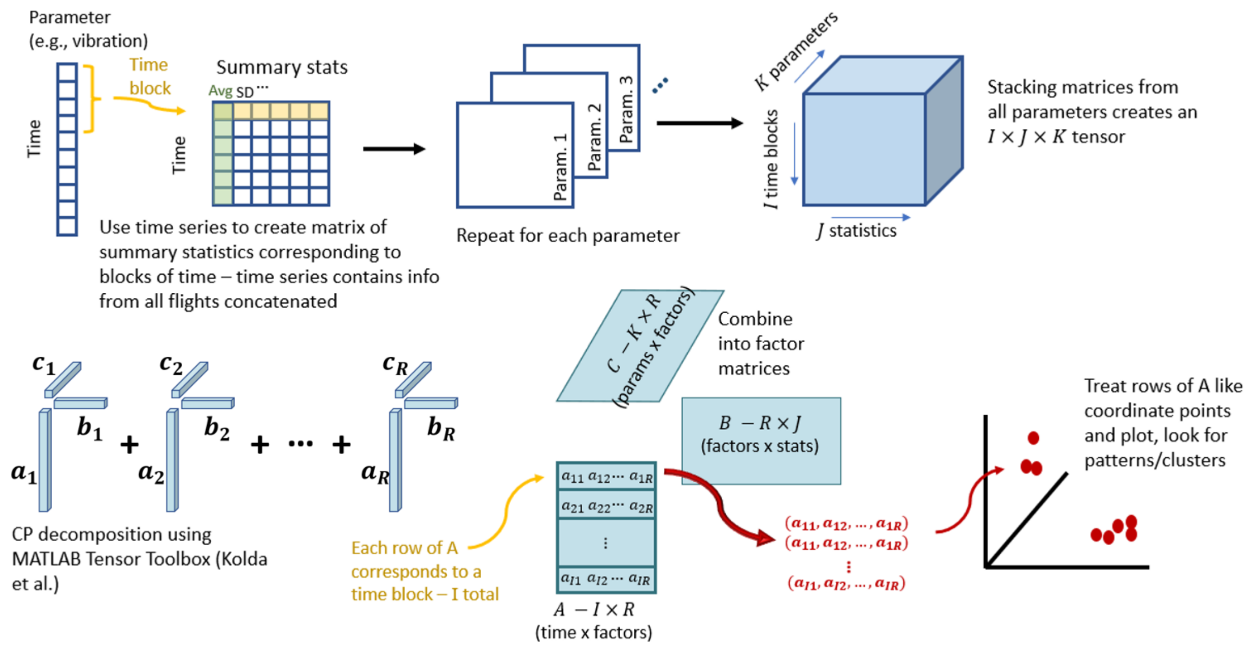

Fig. 4 ITAD flow chart

some or all of these were used throughout our analyses. In particular, each time block has a corresponding row vector of summary statistics. These row vectors are then concatenated vertically to create a matrix with columns corresponding to summary statistics and rows corresponding to each block of time.

Analogous matrices are created for each parameter of interest, and are then concatenated front to back to create the three dimensional tensor. The result is an $I \times J \times K$ tensor, where I is the number of time blocks, J is the number of summary statistics used, and K is the number of parameters used.

After the tensor is constructed, the CP decomposition is performed using the CP ALS algorithm in the MATLAB *Tensor Toolbox* [18]. A major challenge in this process is determining an appropriate rank for the decomposition. As discussed previously, the rank cannot be computed directly. Instead, following the work of [10], we use the reconstruction fit as a guide to a suitable rank for the decomposition. In this setting, we use the minimum rank required to achieve a 90% reconstruction fit. This rank varied depending on the dimensions of the tensor – i.e., the number of time blocks, summary statistics, and parameters used.

For our analysis, we focus on the matrix **A**, as the rows of this matrix correspond directly to different blocks of time in the flights, with each component in the row corresponding to each factor in the CP decomposition. In particular, this means we know which rows correspond to which flights. Treating each row in **A** as a coordinate point, we plot these on coordinate axes. Since in most cases the tensor required a decomposition of rank $R > 3$, MATLAB's gplotmatrix was used to create pairwise plots of the factors.

As mentioned, the focus was initially placed on **A** because each row corresponds to specific segments of time within each flight, so if an anomaly is occuring in the data set, we can then see what point in time (or more generally which flight) it corresponds to. Moreover, since a component of the tensor $\mathcal{X}$ is computed as

$$x_{ijk} = \sum_{r=1}^{R} a_{ir} b_{jr} c_{kr},$$

the elements of **A** represent comprehensive characteristics across all the parameters used in the tensor, enabling the analysis of all used parameters at once.

We note some interesting behavior in this method as new data are incorporated into the tensor. Due to the normalization being based on the maximum values across all flights, the values in the tensor can change when new points are added to the time series. In addition, the tensor decomposition process means that the values in one row of **A** are dependent on values in the other rows of **A**, so changing values or introducing new values impacts previously existing values. While perhaps not intuitive, it does not inherently detract from this analysis as a key advantage of working with tensors is the ability to accentuate the data's relationship to other data along a given dimension.

IV. Experimental Flight Data

In this section, we give an overview of the data used in these analyses. The data were collected by faculty and students at the University of Notre Dame as part of an ongoing effort to create a large data set consisting of a wide range of trajectories flown by quadcopters. The data collection is ongoing, and the team at Notre Dame has communicated their intentions to continue expanding the data set until its release in December 2023. The data set used in this analysis was from the flights performed in summer 2023.

At that point in time, there were data from 23 flights available using 5 different quadcopters labeled "red", "green", "orange", "purple", and "aqua". Specific details on the aircraft were not available. These flights included 10 different trajectories such as straight legs, sawtooths, circles, triangles, and other shapes. Parameters tracked during each of the flights, included GPS, IMU data from three separate sensors, vibration, battery information such as current, voltage, and temperature, as well as metrics for fault detection such as propeller imbalance. Also available for each flight were the average wind speed and direction as well as wind gust, both in knots. Due to biases present in attitude information, the data for roll, yaw, and pitch in each flight were appropriately rescaled and centered.

Of the 23 flights, six experienced at least one anomaly. Four of the flights saw brief losses in communication that resulted in the aircraft stopping to hover before either regaining contact and continuing with the flight or having manual control taken for the remainder of the flight; these were flights 3, 4, 5, and 12. In the case of flights 3, 5, and 12, it is straightforward to ignore the impact of these difficulties by trimming the data set to exclude the portion where the aircraft hovered. One flight, flight 2, experienced a change in the control settings that resulted in the aircraft drifting off course. However, two anomalies were of particular interest in this analysis – flight 1 had an excess payload and flight 5 had unusually strong wind gusts.

Thus, we focus on flights 1, 3, 5, 8, 12, 22, and 23. Flights 1 and 3 flew the triangle trajectory shown in Fig. 5a; these flights used the "red" and "green" aircraft, respectively, and lasted approximately 5 minutes. Flights 5, 8, 12, 22, and 23 all flew the triangle trajectory shown in Fig. 5b. Flights 5, 12, and 23 used the "purple" aircraft, while flight 8 used the "orange" aircraft, and flight 22 used the "aqua" aircraft; each of these lasted approximately 4 minutes. Table 1 summarizes the aircraft, trajectory, wind speed and direction, wind gust, and any anomalies for each flight.

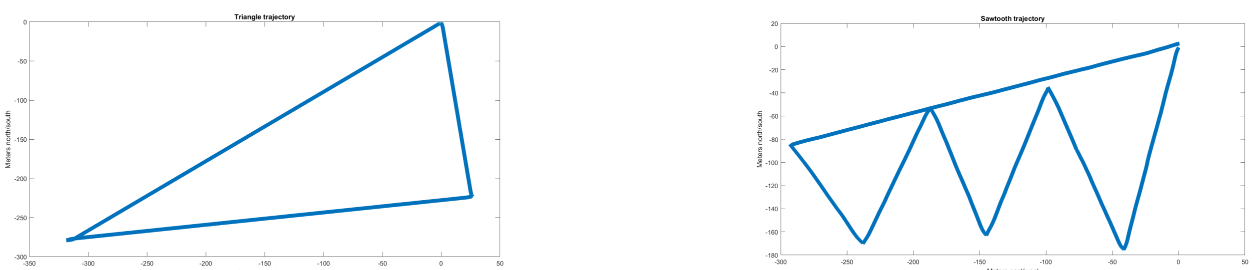

(a) Triangle trajectory: Flights 1 & 3.

(b) Sawtooth trajectory: Flights 5, 8, 12, 22, & 23.

Fig. 5 Trajectories of flights studied.

V. ITAD Application & Results

We begin with flights 1 and 3. For our initial analysis, these flights were broken into 30 second segments, for a total of 10 time segments per flight. The parameters used were vibration, propeller imbalance, velocity in the NED frame, current, velocity, roll, pitch, and yaw, for a total of 10 parameters. The statistics used in the first construction were average, standard deviation, energy, skewness, and quartiles (minimum, lower quartile, median, upper quartile, and maximum) for a total of 9 statistics. The resulting tensor was $20 \times 9 \times 10$ (time $\times$ statistics $\times$ parameters) and required a rank 20 decomposition. Fig. 6 contains the matrix plot of the rows of the columns of $\mathbf{A}$. Since the rank of the decomposition was so high, here we only show the plots of the first ten factors. For example, in the fifth row and third column, the fifth factor is graphed against the third factor, with the third factor along the x axis and the fifth factor along the y axis. We note that the matrix plot is symmetric and that the subdiagonal plots are the same as the superdiagonal

Table 1 Flight summaries.

Flight	Aircraft	Trajectory	Wind Speed (knots)	Wind Gust (knots)	Notes
Flight 1	Red	Triangle	8.26 SW	N/A	Excess payload
Flight 3	Green	Triangle	5.4 SW	10	
Flight 5	Purple	Sawtooth	8 S	18	Strong wind gust
Flight 8	Orange	Sawtooth	8.7SW	12	
Flight 12	Purple	Sawtooth	8.7 NW	10.5	
Flight 22	Aqua	Sawtooth	5 NE	6	
Flight 23	Purple	Sawtooth	6 E	10	

plots with the axes swapped. Across these plots, we can see some differences in behavior of the points corresponding to the two flights. Most notably, in the eighth column, we see that the points corresponding to flight 1 tend to appear on the right and the points corresponding to flight 3 tend to appear on the left.

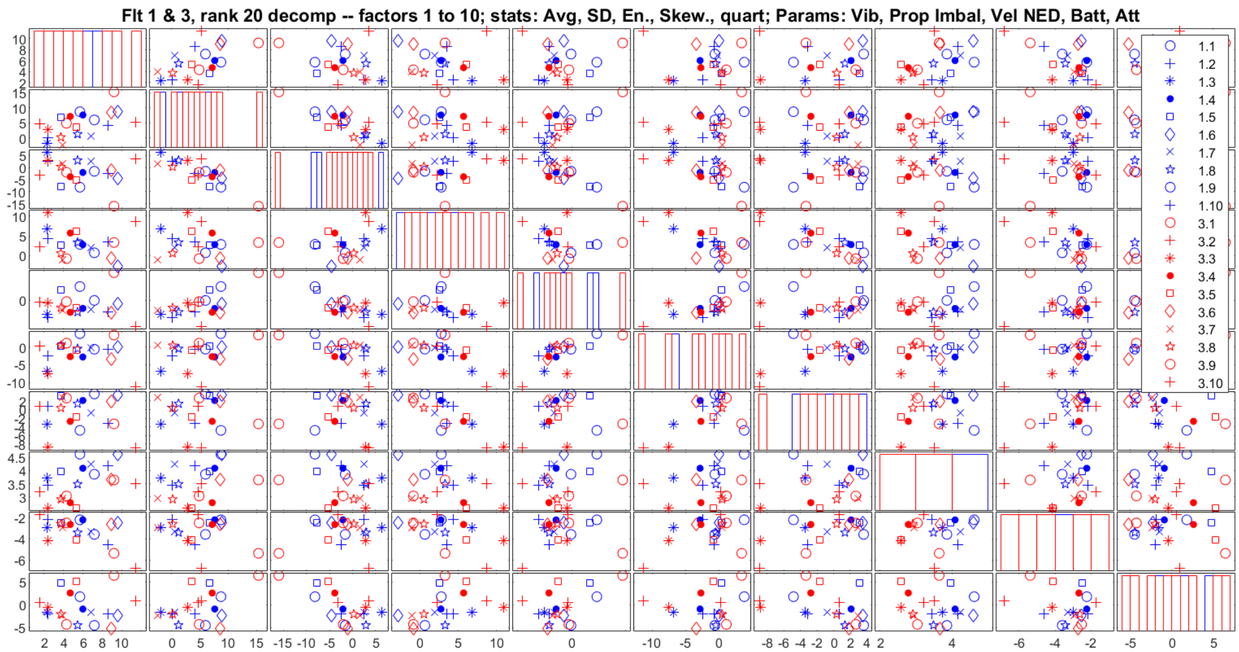

Fig. 6 Flights 1 & 3
Parameters: Vibration, propeller imbalance, velocity (NED), current, voltage, roll, pitch, yaw
Statistics: Average, standard deviation, energy, skewness, minimum, lower quartile, median, upper quartile, maximum

It was decided to reduce the quantity of trajectory-specific data in order to minimize masking of parameters that would contain distinguishing characteristics such as vibration and battery information. Fig. 7 shows the plot corresponding to a tensor created from flights 1 and 3, with the same time segments, but using vibration, velocity north, current, voltage, and roll, and using the statistics average, standard deviation, energy, minimum, and maximum. This tensor was $20 \times 5 \times 5$ and used a rank 7 decomposition. The matrix plot shown in Fig. 7 includes all 7 factors. It is clear across multiple factors that there is separation between the points corresponding to flight 1 and flight 3. Recall that flight 1 had experienced the excessive payload, which resulted in higher vibrations and current draw, and this approach was able to separate between the anomalous flight 1 and the nominal flight 3.

We now consider results from flights 5, 12, and 23 which all used the "purple" aircraft and the sawtooth trajectory.

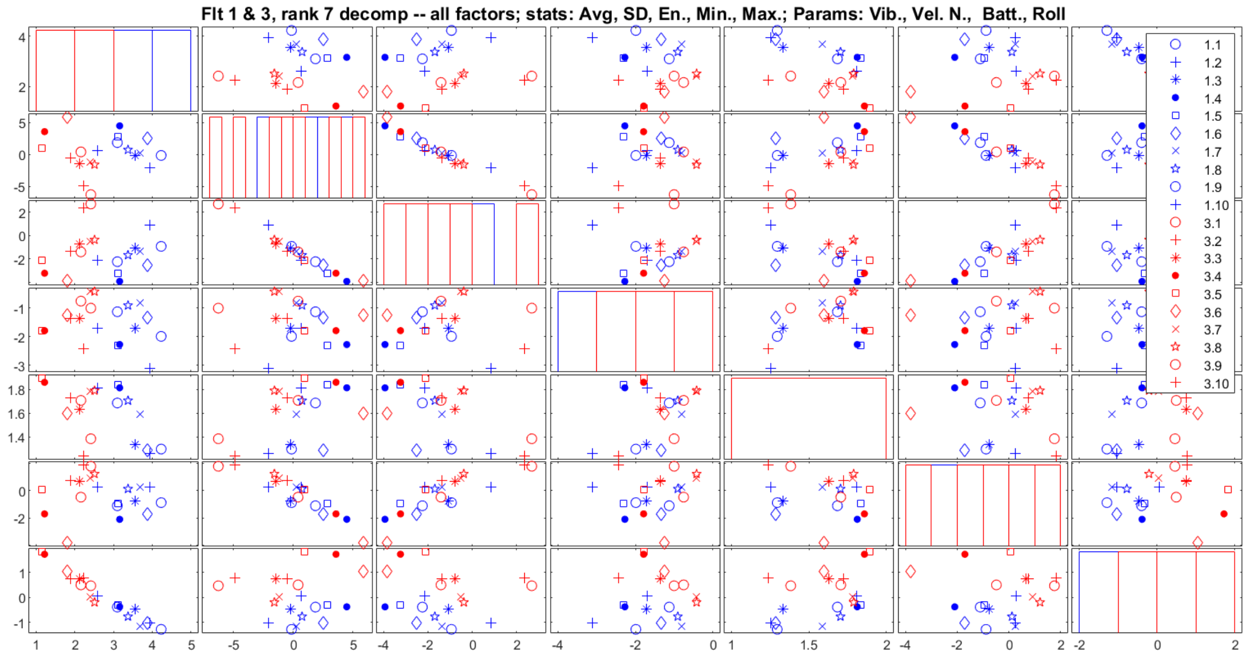

Fig. 7 Flights 1 & 3
Parameters: Vibration, velocity (N), current, voltage, roll
Statistics: Average, standard deviation, energy, minimum, maximum

Fig. 8 shows the results from using the parameters vibration, velocity north, current, voltage, and roll, and the statistics average, standard deviation, energy, minimum, and maximum. The tensor constructed from this data was $24 \times 5 \times 5$ and gave a rank 7 decomposition. In Fig. 8 we can see that the points from flight 5 tend to be more spread out and slightly offset from the corresponding points from flight 12 and flight 23, especially in the first, fourth, and fifth column.

We can further reduce the parameters, including only vibration, velocity north, current, and voltage. This tensor was $24 \times 5 \times 4$ and had a rank 5 decomposition. In Fig. 9, while there are still no distinct clusters, it is clear that the points from flight 5 behave differently than the points from flights 12 and 23, being more spread out and offset from those corresponding to the other two flights.

Finally, we consider tensors constructed from flights 5, 12, and 23 broken into 15s time blocks. This division isolates the turns from the rest of the flight, thus enabling each time segment to correspond to a short straight leg in the flight and minimizing masking that could occur due to changes in direction during flight. In this case, each flight had 16 time blocks, we use the parameters vibration, velocity north, current, voltage, and roll, along with the usual statistics. The result is a tensor that is $48 \times 5 \times 5$, which had a rank 6 decomposition. Fig. 10 shows the plot of the factor matrix $\mathbf{A}$, omitting the points corresponding to time segments containing turns. The points clearly separate by flight, and the small clusters for each flight also correspond to the direction the aircraft was flying, likely due to the parameter of velocity north. Note that the small clusters corresponding to flight 5 are separate from the small clusters corresponding to flights 12 and 23, indicating that this approach is able to isolate anomalous flights.

VI. Conclusion

In this analysis, we have explored the implementation of a tensor-based analysis incorporating multiple parameters to detect anomalies during quadcopter flight. In the application to flights 1 and 3, where flight 1 had experienced excessive payload, this method was successful at isolating flight 1 from flight 3. In the application to flights 5, 12, and 23, where flight 5 had experienced excessive wind gusts, we saw clear distinctions in the behavior of the points corresponding to flight 5. Moreover, the results from working with shorter time segments indicate clear differences detected between the flights. We also note that this approach is very general and can easily be adapted to other settings for anomaly detection. Next steps will include additional approaches to tensor construction capable of isolating highlighting parameter-focused

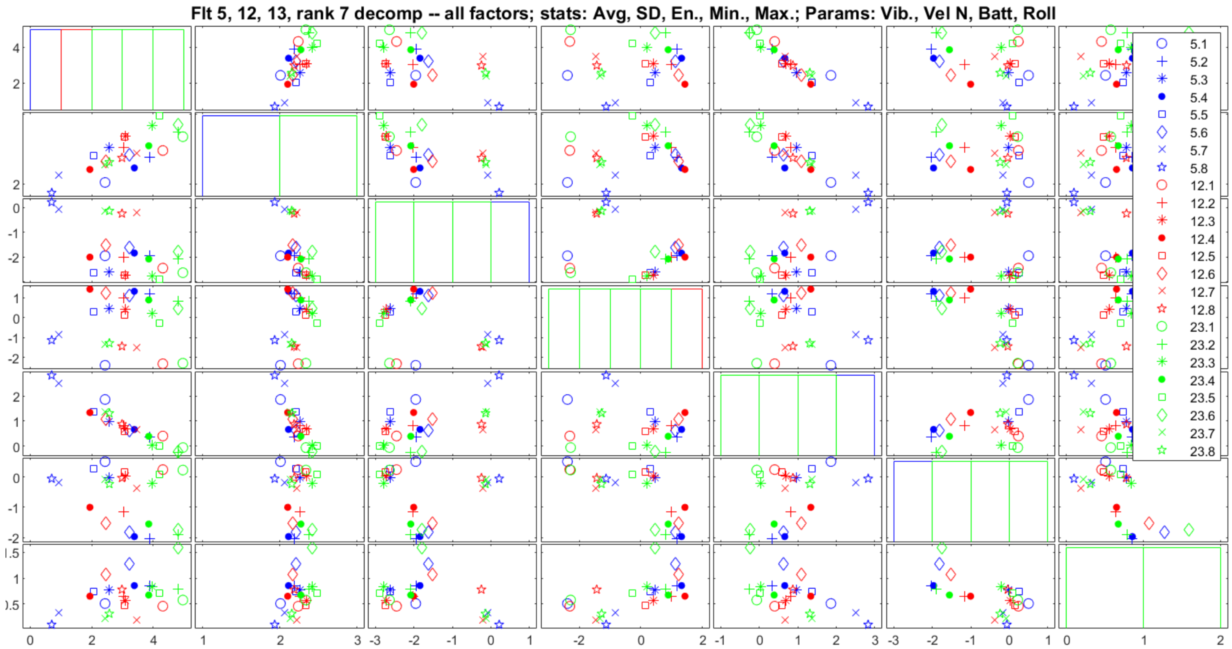

Fig. 8 Flights 5, 12, & 23
Parameters: Vibration, velocity (N), current, voltage, roll
Statistics: Average, standard deviation, energy, minimum, maximum

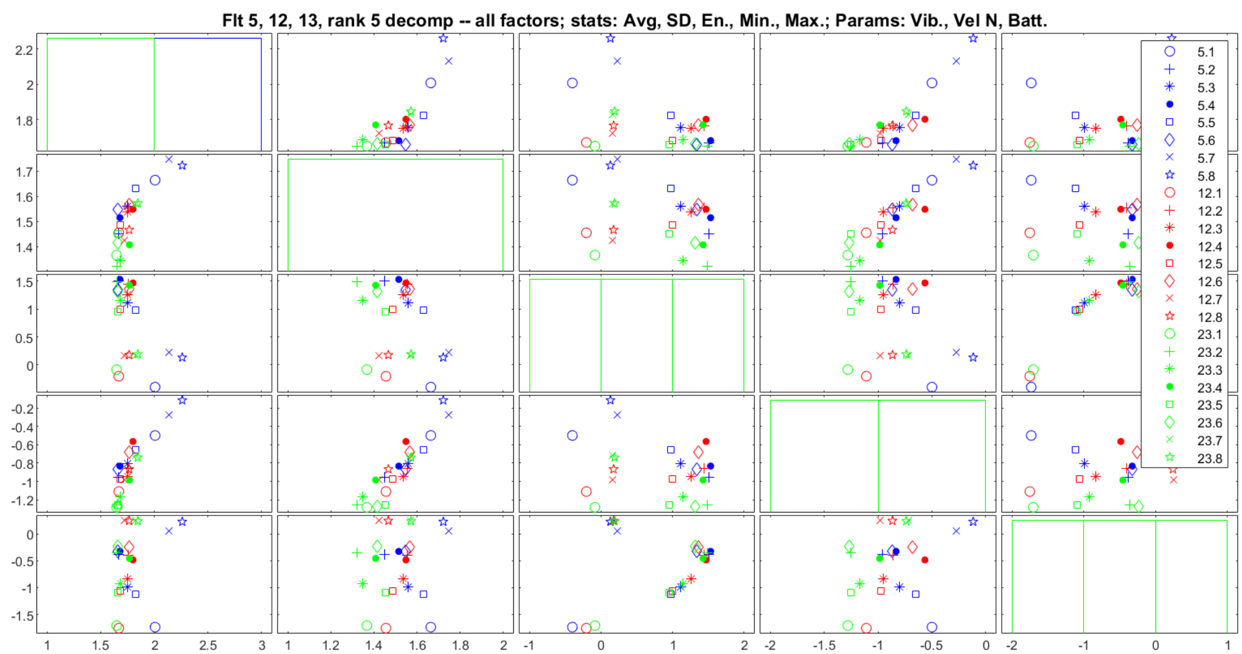

Fig. 9 Flights 5, 12, & 23
Parameters: Vibration, velocity (N), current, voltage
Statistics: Average, standard deviation, energy, minimum, maximum

information, as well as isolating specific segments of flight such as take off and landing. It would also be beneficial to apply clustering and other machine learning approaches to identifying points corresponding to anomalous flights.

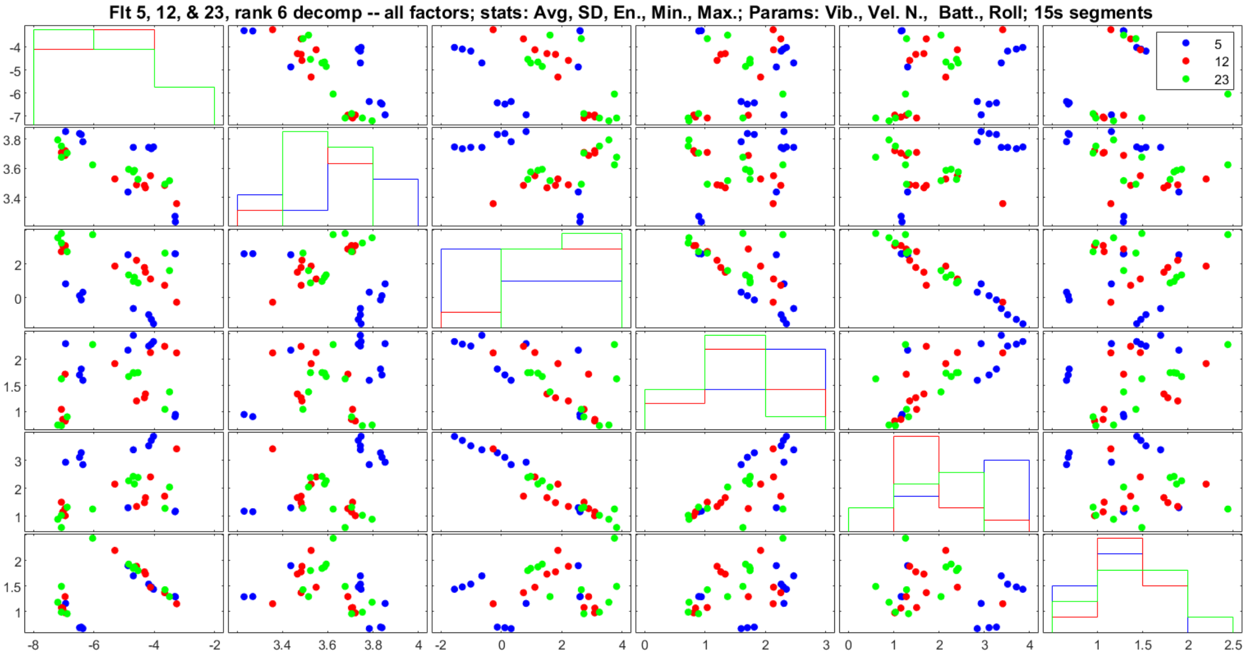

Fig. 10 Flights 5, 12, & 23; 15s time blocks
Parameters: Vibration, velocity (N), current, voltage, roll
Statistics: Average, standard deviation, energy, minimum, maximum

Acknowledgments

This work was supported by the System-Wide Safety (SWS) project under the Airspace Operations and Safety Program within the NASA Aeronautics Research Mission Directorate (ARMD). The authors would like to thank Jane Huang and Walter Scheirer from University of Notre Dame for leading the UAV flight experiments conducted at Notre Dame under NSF award number:1931962 and sharing the data for analysis.

References

[1] Al-Badour, F., Sunar, M., and Cheded, L., "Vibration of Rotating Machinery Using Time-Frequency Analysis and Wavelet Techniques," *Mechanical Systems and Signal Processing*, Vol. 25, 2011, pp. 2083–2101.

[2] Bondyra, A., Gasior, P., Gardecki, S., and Kasiński, A., "Fault diagnosis and condition monitoring of UAV rotor using signal processing," *2017 Signal Processing: Algorithms, Architectures, Arrangements, and Applications (SPA)*, IEEE, 2017, pp. 233–238.

[3] Ghalamchi, B., Jia, Z., and Mueller, M. W., "Real-Time Vibration-Based Propeller Fault Diagnosis for Multicopters," *IEEE/ASME Transactions on Mechatronics*, Vol. 25, No. 1, 2020, pp. 395–405. https://doi.org/10.1109/TMECH.2019.2947250.

[4] Ghalamchi, B., and Mueller, M., "Vibration-Based Propeller Fault Diagnosis for Multicopters," *2018 International Conference on Unmanned Aircraft Systems (ICUAS)*, 2018, pp. 1041–1047. https://doi.org/10.1109/ICUAS.2018.8453400.

[5] Banerjee, P., Okolo, W. A., and Moore, A. J., "In-Flight Detection of Vibration Anomalies in Unmanned Aerial Vehicles," *ASME J Nondestructive Evaluation*, Vol. 3, No. 4, 2020.

[6] Banerjee, P., Ghimire, R., and Hale, E., "Vibration Anomaly Detection by Clustering in Unmanned Aerial Vehicles," *Proceedings of the AIAA Aviation Forum*, 2023.

[7] Bektash, O., and la Cour-Harbo, A., "Vibration Analysis for Anomaly Detection in Unmanned Aircraft," *Annual Conference of the PHM Society*, 2020.

[8] Cabahug, J., and Eslamait, H., "Failure Detection in Quadcopter UAVs Using K-Means Clustering," *Sensors*, Vol. 22, No. 6037, 2022.

[9] Liu, F. T., Ting, K. M., and Zhou, Z.-H., "Isolation forest," *2008 eighth ieee international conference on data mining*, IEEE, 2008, pp. 413–422.

[10] Shin, Y., Lee, S., Tariq, S., Lee, M. S., Jung, O., Chung, D., and Woo, S. S., "ITAD: Integrative Tensor-Based Anomaly Detection System for Reducing False Positives of Satellite Systems," *Proceedings of the 29th ACM International Conference on Information & Knowledge Management*, Association for Computing Machinery, 2020, p. 2733–2740.

[11] Mohamed, A., Marino, M., Watkins, S., Jaworski, J., and Jones, A., "Gusts Encountered by Flying Vehicles in Proximity to Buildings," *Drones*, Vol. 7, No. 1, 2022, p. 22. https://doi.org/10.3390/drones7010022, URL http://dx.doi.org/10.3390/drones7010022.

[12] Lei, Y., Huang, Y., and Wang, H., "Effects of Wind Disturbance on the Aerodynamic Performance of a Quadrotor MAV during Hovering," *Journal of Sensors*, Vol. 2021, 2021.

[13] Kolda, T. G., and Bader, B. W., "Tensor Decompositions and Applications," *SIAM Review*, Vol. 51, 2009, pp. 455–500.

[14] stad, J. H., "Tensor rank is NP-complete," *Nournal of Algorithms*, Vol. 11, No. 4, 1990, pp. 644–654.

[15] Hitchcock, F. L., "The Expression of a Tensor or Polyadic as a Sum of Products," *J. Math. Phys.*, Vol. 6, 1927, pp. 164–189.

[16] Carroll, J. D., and Chang, J. J., "Analysis of Individual Differences in Multidimensional Scaling via an N-way Generalization of "Eckart-Young" Decomposition," *Psychometrika*, Vol. 17, 1970, pp. 283 – 319.

[17] Harshman, R. A., "Foundations of the PARAFAC Procedure: Models and Conditions for an 'Explanatory' Multi-Modal Factor Analysis," *UCLA Working Papers in Phonetics*, Vol. 16, 1970, pp. 1–84.

[18] Bader, B. W., Kolda, T. G., et al., "MATLAB Tensor Toolbox Version 3.1," Available online, Jun. 2019. URL https://www.tensortoolbox.org.